Advanced Radio Frequency Energy Harvesting with Power Management from Multiple Sources for Low Power Sensors and Mobile Charging Applications

Manee Sangaran[1, *], Agileswari Ramasamy[2], and Norashidah Md Din[1]

Abstract—A complete energy harvesting system via Radio Frequency (RF) is designed in a broadcast station where multiple frequency sources are readily available. These frequency sources are the Intermediate Frequency (IF), 70 MHz, Wi-Fi frequency band, 2.4 GHz, and the Ku-band frequency, 13 GHz. The RF source via the Wi-Fi band (2.4 GHz) is harvested via a microstrip patch antenna designed with its matching network. The harvested RF energy is transformed into usable DC power via an 8-stage Villard voltage doubler circuit. The DC power is managed by a power management system handled by the BQ25570 circuit which gives a regulated output of 3 V, powers up a low power motion sensor, and charges a battery at the same time. This system comes with a backup source which is the battery and able to take over the system in case the incoming RF signal fails. The RF energy harvested from the IF 70 MHz and Ku-band at 13 GHz is derived from coupler outputs which are available in broadcast stations, transmission lines, etc. Both these RF signals are converted to DC signals via a 5-stage Villard voltage doubler circuit with different matching networks. The DC power is managed by a power mux via the TPS2122 which selects the highest available power. Over the years, no works on RF harvesting have focused on smart phone charging as its application, due to the limitation in power availability. This work strives to provide enough power to charge phones and effectively gives a 5 V output to charge smart phones with a charging current of 0.5 A which is similar to a USB charging port.

1. INTRODUCTION

During the recent times, a number of research works have been done on RF energy harvesting whereby RF energy from surroundings is captured and converted into DC power for low power applications [1]. Various methods of RF energy scavenging have been discovered over the years to make use of this readily available energy source. The core idea of this harvesting method is that the RF energy is scavenged with a microstrip patch antenna and transformed into DC power via some sort of rectifier circuit. The DC is then regulated and managed by a power management circuit [2]. This method of energy harvesting best works on networks with limited power. One of such networks would be wireless sensor networks. A major drawback here is that wireless sensor networks have a limited battery lifetime, and this energy harvesting method can be utilized to power up these sensors in return eliminating the usage of batteries [3]. Most of the researches have covered on capturing RF signals from the ambience and at low frequency. This work extensively concentrates on harvesting RF energy from the ambience and as well as low and high frequency sources which are the Wi-Fi 2.4 GHz, IF 70 MHz, and also Ku-band 13 GHz. For this, a broadcast station is chosen, and the RF sources available here are harvested and converted into DC power. The same concept can be applied to other broadcast stations or transmission

sites, whereby RF energy is readily available [4]. No research has been done via this harvesting method, and this work successfully harvests RF energy from multiple sources to power up a low power sensor and is also used to charge smart phones. Results and analysis are discussed based on the RF energy harvesting system designed.

2. THEORETICAL FRAMEWORK

A basic RF energy harvesting system would have an antenna, a matching network, and some sort of rectifier circuit for energy conversion. RF energy is captured via the antenna, and a matching network is included to ensure the impedances match. Maximum power transfer is observed. This RF energy is then converted into DC power. The Wi-Fi energy is easily accessible in many areas nowadays. Since this work focuses in a broadcast station, the Wi-Fi energy will be captured from the data center rooms as well as broadcast equipment rooms as the Wi-Fi signal strength is measured to be high in these areas. Figure 1 depicts the RF energy harvesting prototype designed to capture energy from the 2.4 GHz frequency band.
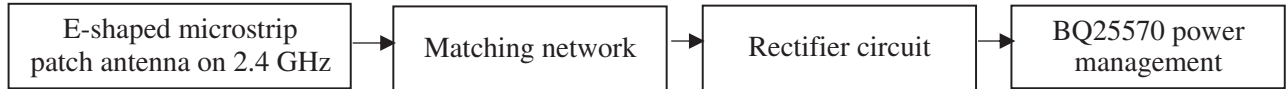
E-shaped microstrip patch antenna on 2.4 GHz	→	Matching network	→	Rectifier circuit	→	BQ25570 power management

Figure 1. Signal flow for 2.4 GHz Wi-Fi frequency band harvesting system.

To harvest the signals from 2.4 GHz, an E-shaped microstrip patch antenna was designed. The impedance of the antenna and the RF to DC circuit is matched via a matching network circuit to ensure proper power transfer. An 8-stage Villard voltage doubler circuit is designed to transform the RF to usable DC. The DC output is then connected to the Texas Instruments BQ25570 circuit. The power management circuit boosts the input DC power and supplies a regulated output to the load and charges a rechargeable battery simultaneously. When there is no incoming RF or DC supply, the battery will continue to provide power to the load. This regulated DC output from the power management circuit is utilized to power up a motion sensor.

Next, the RF energy is derived from the uplink transmission path in the broadcast station. There are two stages of harvesting in the uplink transmission path which consists of the low frequency and high frequency. The low frequency is derived from the IF 70 MHz, and the high frequency is derived from the Ku-band uplink transmission frequency which is at 13 GHz. Ku-band is the most commonly used frequency range for direct-to-Home broadcast transmission in Malaysia. This work will be the first to explore energy harvesting in a broadcast environment and also first of the very few works to harvest energy from Ku-band frequency range and utilized for smart phone charging application. Figure 2 depicts the general signal flow of an uplink transmission path.
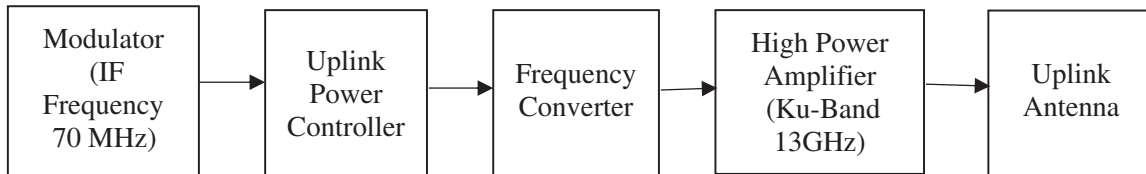
Modulator (IF Frequency 70 MHz)	→	Uplink Power Controller	→	Frequency Converter	→	High Power Amplifier (Ku-Band 13GHz)	→	Uplink Antenna

Figure 2. Uplink transmission signal flow.

A modulator is used to modulate the information and data into a carrier signal for transmission which operates on IF frequency 70 MHz. The modulator has a coupler output which can be used for energy conversion as this output will not be utilized for transmission. Most equipment on a transmission path will have coupler outputs for the purpose of monitoring and can be utilized for energy harvesting as the coupler outputs will not be used most of the time. In this case, the modulator coupler output

gives an IF 70 MHz at a constant power level of +10 dBm. Since the RF signal is readily available, an antenna will not be required, and the RF signal can be fed directly into the rectifier circuit to produce the DC power.

The uplink power controller is responsible for controling the transmission power to the satellite. Since the transmission is on Ku-band frequency, which is prone to rain, a higher transmission power is required during rain to mitigate rain fade and ensure that the RF signal reaches the satellite. The frequency converter is used to convert the IF 70 MHz frequency to Ku-band frequency. The Ku-band frequency is then fed to the High-Power Amplifier (HPA) which is used to boost the uplink power in case of rain. The HPA's output power varies based on the weather condition and will boost to 2000 W in case of rain which will be controlled by the uplink power controller. The HPAs have a coupler output as well which gives the Ku-band 13 GHz output which will be used for harvesting. The power level from this coupler was measured to be at +0 dBm during clear sky weather conditions and can go up to +30 dBm during rain.

The drawback from harvesting this 13 GHz output is that during energy conversion to DC, it faces a large amount of loss due to its high frequency nature. This is only observed during clear sky weather conditions whereby the power level of the HPA coupler output is at +0 dBm. However, a very high-power level is observed during rain, and despite the loss during energy conversion, a large amount of DC was able to be produced. Hence, the IF and Ku-band energy is harvested simultaneously, and a smart power management is designed to select the higher output. Figure 3 shows the system design to harvest the IF 70 MHz and Ku-band 13 GHz frequency range.
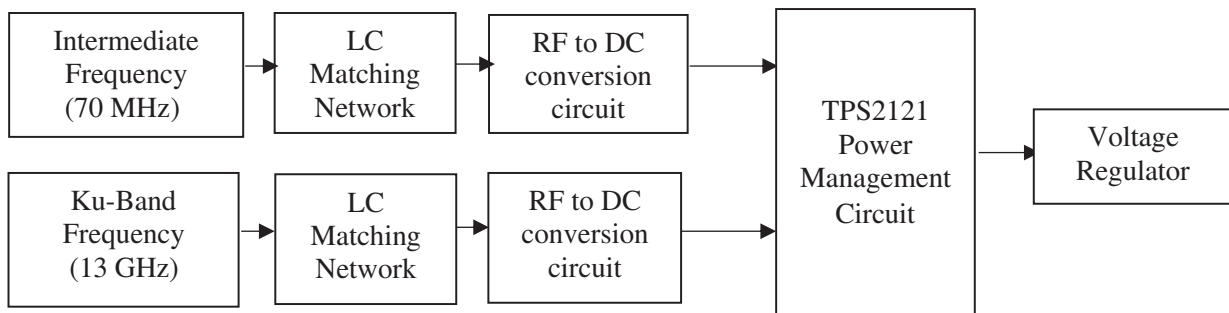

Figure 3. Signal flow for IF 70 MHz and Ku-band 13 GHz frequency band harvesting system.

A 5-stage Villard voltage doubler circuit is designed to transform the RF to DC. Both the outputs from the IF 70 MHz and Ku-band 13 GHz are connected to the TPS2121 power management interface. As mentioned above, the Ku-band frequency produces very low DC power during clear sky weather conditions. During this period, the DC power from the IF 70 MHz circuit will be utilized for the mobile charging. When it starts to rain, the DC power harvested from the Ku-band frequency will be used instead since it produces more DC power and enables a faster charging rate than the IF 70 MHz frequency. This selection will be managed by the TPS2121, and it is fully automated. The DC output is fed into a voltage regulator to produce a regulated 5 VDC for smart phone charging.

3. DESIGN AND ANALYSIS OF RF HARVESTING VIA WI-FI 2.4 GHZ

This section discusses the circuit design and analysis for the RF harvesting via W-Fi 2.4 GHz.

3.1. Microstrip Patch Antenna

As depicted in Figure 1, an E-shaped microstrip patch antenna was designed to capture RF energy in the 2.4 GHz frequency band. The Computer Simulation Technology (CST) program was used to design the antenna, and parameter changes were done to achieve optimum bandwidth and return loss. This E-shaped patch antenna with a thickness of 1.6 mm and dielectric constant value of 4.3 was fabricated on an FR4 substrate. A partial ground plane is designed instead of the conventional full ground plane

to achieve better performance on the antenna. Using Equation (1), the antenna's effective dielectric constant ε_{reff} was calculated [5].

For $W/h > 1$

$$\varepsilon_{reff} = \frac{\varepsilon_r + 1}{2} + \frac{\varepsilon_r - 1}{2}\left[1 + 12\frac{h}{W}\right]^{-1/2} \tag{1}$$

The length extension, ΔL, is defined as a function of the width-to-height ratio (W/h) and also the effective dielectric constant ε_{reff}. The length extension ΔL is basically the dimensions of the patch along its length that is caused by fringing effects on the xy-plane. The center frequency (f_r) of the antenna is associated with the length (L) of the antenna which is calculated using Equations (2) and (3)

$$L = \frac{\tau}{2} - \Delta L = \frac{1}{2f_r\sqrt{\mu_0\varepsilon_0}\sqrt{\varepsilon_{reff}}} - 2\Delta L \tag{2}$$

where

$$\Delta L = 0.412 X h X \frac{(\varepsilon_{reff} + 0.3)\left(\dfrac{W}{h} + 0.264\right)}{(\varepsilon_{reff} - 0.258)\left(\dfrac{W}{h} + 0.8\right)} \tag{3}$$

The antenna's bandwidth and impedance are associated with the width (W). It is defined in terms of the substrate dielectric constant and the resonant frequency of the antenna where v_0 is the speed of light. Equation (4) was used to determine the width.

$$W = \frac{1}{2f_r\sqrt{\mu_0\varepsilon_0}}\sqrt{\frac{2}{\varepsilon_r + 1}} = \frac{v_0}{2f_r}\sqrt{\frac{2}{\varepsilon_r + 1}} \tag{4}$$

The microstrip patch antenna equations were used to obtain the dimensions of the antenna, and two horizontal slots were introduced on the patch for fringing effects in order to optimize the performance of the antenna [6]. The feed line was strategically placed to ensure that an efficient return loss was achieved through this design. An SMA connector is placed at the output of the antenna in order to test the performance of the antenna.
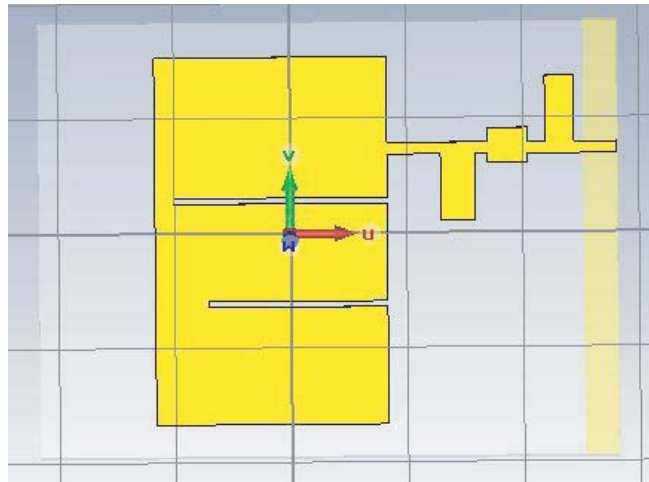
Figure 4 shows the design of the antenna on CST.

Figure 4. Design of E-shaped microstrip patch antenna on CST.

The measurements of the antenna were computed using the antenna equations as discussed above. Two slots were introduced to induce fringing effects, and the designed antenna was optimized to obtain the desired return loss and antenna bandwidth. Table 1 depicts the dimensions of the antenna.

Table 1. Measurements of E-shaped microstrip patch antenna.

Element	Parameter		Measurement (mm)
Patch Antenna	Width		32
	Length		20
E-Slot	Slot 1	Width	0.5
		Length	18
	Slot2	Width	0.5
		Length	15
Feed Line	Width		1
	Length		16.5
Ground Plane	Width		38
	Length		0.3

The input impedance of the rectifier circuit was measured using a network analyzer, and it was measured to be at $13.72 - j19.14$. An impedance matching network with a source of $50\,\Omega$ was designed to match the load of $13.72 - j19.14$. This was done via the Smith chart utility available on Agilent Design System (ADS) software. The transmission line calculator was then utilized to obtain the microstrip parameters as shown in Figure 5.
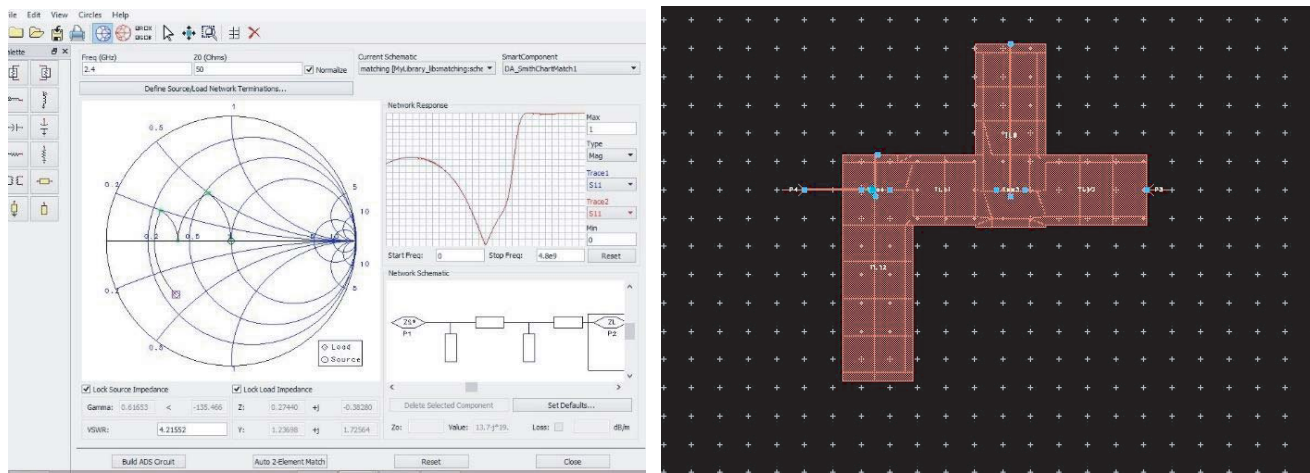

Figure 5. Impedance matching network design via ADS & transmission line calculator.

The microstrip patch antenna together with its matching network was fabricated on an FR4 substrate and tested under certain conditions. The fabricated patch antenna is shown in Figure 6.

3.2. RF to DC Conversion Circuit

An 8-stage Villard voltage doubler circuit is designed to transform the RF to DC using the Agilent HSMS-282 diodes [7]. These diodes were chosen due to their low forward voltage nature [8]. The NI Multisim software was used to design and simulate the RF to DC circuit. Figure 7 shows a single stage of the voltage doulber circuit.

Each stage of the voltage doulber circuit can be depicted as a battery with an open circuit output voltage V_0 and also an internal resistance R_0. The output voltage V_{out} is expressed as in Eq. (5) with R_L as the load resistance.

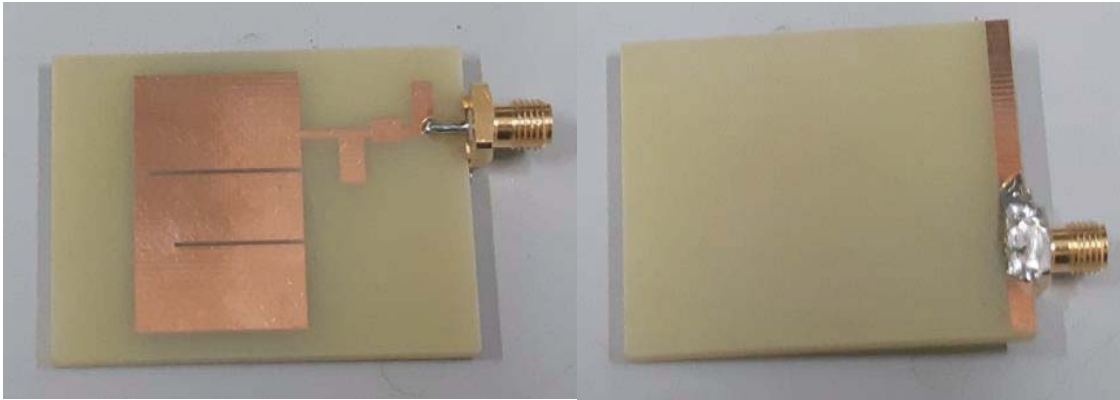$$V_{out} = \frac{V_0}{R_0 + R_L} R_L \tag{5}$$

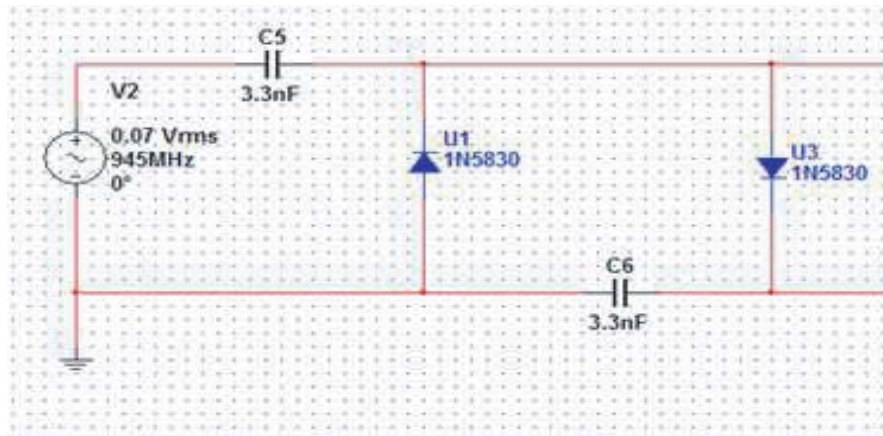**Figure 6.** Fabricated E-shaped microstrip patch antenna together with the partial ground plane.

Figure 7. Single stage voltage doulber circuit.

These circuits are connected into series with a load resistance R_L. Then, V_{out} is obtained as in Eq. (6) where n is the number of stages of these circuits which are connected in series.

$$V_{out} = \frac{nV_0}{nR_0 + R_L}R_L = V_0\frac{1}{\dfrac{R_0}{R_L} + \dfrac{1}{n}} \tag{6}$$

The rectifier components are as shown in Table 2. The circuit was fabricated on an FR4 substrate with two SMA connectors as input and output for testing purposes. Figure 8 shows the fabricated rectifier circuit.

Table 2. Rectifier circuit components.

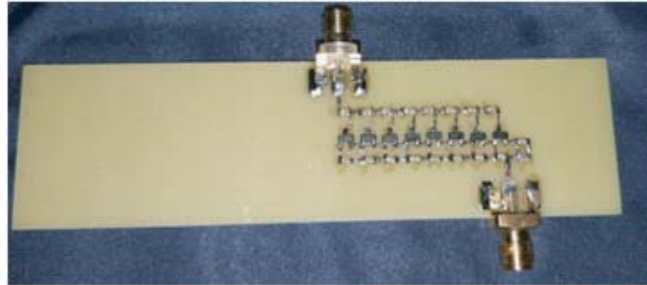| Component	Type
Diodes	Agilent HSMS-282
Stage Capacitor	$100\,\mu F$
Filter Capacitor	$100\,nF$
Load Resistor	$50\,k\Omega$

Figure 8. Fabricated rectifier circuit.

3.3. Power Management

As shown in Figure 9, the Texas Instruments (TI) BQ25570 is incorporated as a power management circuit for this system. The BQ25570 is equipped with an adjustable Maximum Power Point Tracking (MPPT) [9] algorithm which makes sure that the input voltage does not decrease under 50% or 80% of the earlier open circuit voltage. The input voltage (VIN) is sampled based on the voltage reference (VREF_SAMP). Values of external resistors (R_{OC1} & R_{OC2}) were calculated to ensure that the exact ratio for MPPT is optimized based on Equation (7) as below:

$$VREF_{\text{SAMP}} = VIN_{DC\left(\frac{R_{OC1}}{R_{OC1}+R_{OC2}}\right)} \tag{7}$$

Besides that, the BQ25570 has a regulated boost converter output (V_{OUT}), which will be used to power up the low power sensor. The external resistors (R_{OUT1} & R_{OUT2}) values were calculated to set V_{OUT}
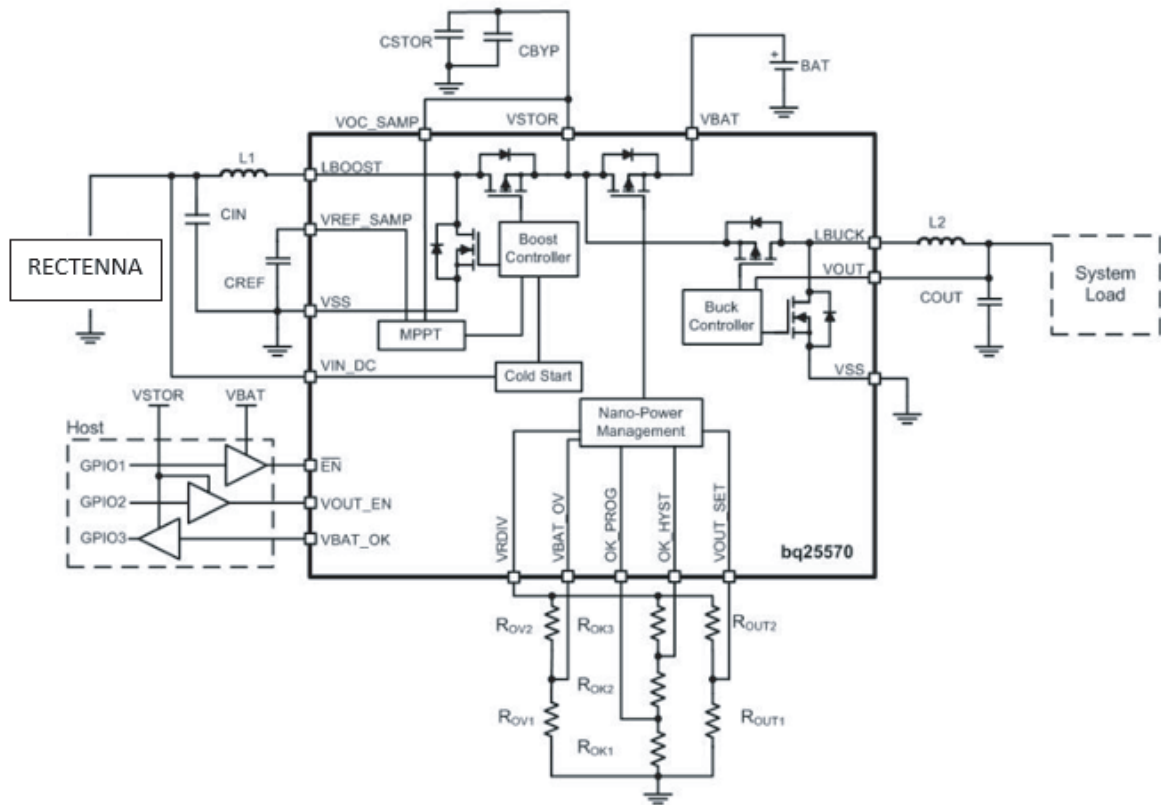

Figure 9. BQ25570 circuitry design.

as 3 V based on Equation (8) where V_{BIAS} is nominally 1.21 V as per datasheet of the BQ255570.

$$V_{OUT} = V_{BIAS} \left(\frac{R_{OUT1} + R_{OUT2}}{R_{OUT1}} \right) \tag{8}$$

The BQ25570 is also programmed to charge a rechargeable battery (V_{BAT}) and at the same time provide a regulated output. The battery has an overvoltage protection whereby charging is stopped in case battery is overcharged. The external resistors ($R_{OV1}\&R_{OV2}$) are calculated based on Equation (9) whereby $V_{BAT_{OV}}$, the overvoltage protection value, is set to 4.2 V.

$$V_{BAT_{OV}} = \frac{3}{2} V_{BIAS} \left(1 + \frac{R_{OV2}}{R_{OV1}} \right) \tag{9}$$

If there is no DC power at the incoming of the circuit, the battery would take over the circuit and provide the regulated output to constantly provide power to the low power sensor. This means that there will be no interruption of power supply to the sensor. The IC also has a very low cold start voltage condition which is 330 mV and is easily doable from RF to DC conversion circuit. The internal capacitor (V_{STOR}) is initially charged up to 4.2 V, which powers up the boost controller. Once V_{STOR} is fully charged, input as low as 100 mV is sufficient to operate the circuit.

The BQ25570 is designed to produce a constant regulated voltage of 3 V. The output of the power management circuit is used to power up the low power motion sensor TIDA-01398. The final fabricated circuit of the BQ25570 is as shown in Figure 10.

Figure 10. Fabricated BQ25570 power management circuit.

4. DESIGN AND ANALYSIS OF RF HARVESTING VIA 70 MHZ AND 13 GHZ

This section discusses the circuit design and analysis for the RF harvesting via 70 MHz and 13 GHz frequency bands.

4.1. RF to DC Conversion Circuit

As shown in Figure 3, two 5-stage voltage doubler circuits were designed to convert RF energy into usable DC which is harvested from the uplink transmission path of a broadcast station [10]. Table 3 shows the components used to design the rectifier circuit.

Table 3. Components on the rectifier circuit for harvesting 70 MHz and 13 GHz signals.

Component	70 MHz	13 GHz
Diodes	Skyworks CLA4601-000	Skyworks SMS7621
Stage Capacitor	0.1 μF	100 μF
Filter Capacitor	100 nF	100 pF
Load Resistor	50 kΩ	50 kΩ

The capacitors were carefully selected based on the input frequency and also the peak voltage rating. The diodes are chosen depending on the input frequency and the maximum RF input power it can withstand. Figure 11 shows the RF to DC conversion circuit fabricated to harvest the 70 MHz and 13 GHz signals.

Figure 11. RF to DC conversion circuit fabricated to harvest the 70 MHz and 13 GHz signals.

4.2. LC Matching Network Circuit

The input impedance of the 70 MHz RF to DC conversion was measured to be at $18.36 - j11.09$ with input power level of $+10$ dBm. The ADS Smith chart utility was used to match the impedance of $50\,\Omega$ to the input impedance $18.36 - j11.09$. The lumped elements [11, 12] are transformed to distributed elements in the matching network using Equations (10) to (12) where the open circuit capacitance (Z_{cap}^{oc}) and impedance (Z_{ind}^{oc}) are calculated:

$$Z_{in}^{oc} = -jZ_0 \cot \beta l = -j50 \cot \beta l \tag{10}$$

where

$$\beta = \frac{2\pi}{\tau} \quad \text{and} \quad \tau = \frac{\tau_0}{\sqrt{\varepsilon_{reff}}}$$

$$Z_{cap}^{oc} = \frac{1}{jWC} \tag{11}$$

$$Z_{ind}^{oc} = jWL \tag{12}$$

From there, the LC circuit was derived and fabricated at the input of the rectifier circuit as shown in Figure 11. Figure 12 shows the impedance matching design for the 70 MHz RF to DC conversion circuit via ADS.

The input impedance of the 13 GHz RF to DC conversion was measured to be at $72.87 - j59.94$. The ADS Smith chart utility was used to match the impedance of $50\,\Omega$ to the input impedance $72.87 - j59.94$. Figure 13 shows the impedance matching design for the 13 GHz RF to DC conversion circuit via ADS.

With the LC impedance matching circuit, a better power transfer from the transmission path to the RF to DC conversion circuit was noticed. The results will be discussed in a greater detail in Section 5.

4.3. Power Management

The TI TPS2121 power mux IC was used to design the power management circuit by feeding both the DC voltages from the RF to DC circuits [13]. The power management circuit will select the input with
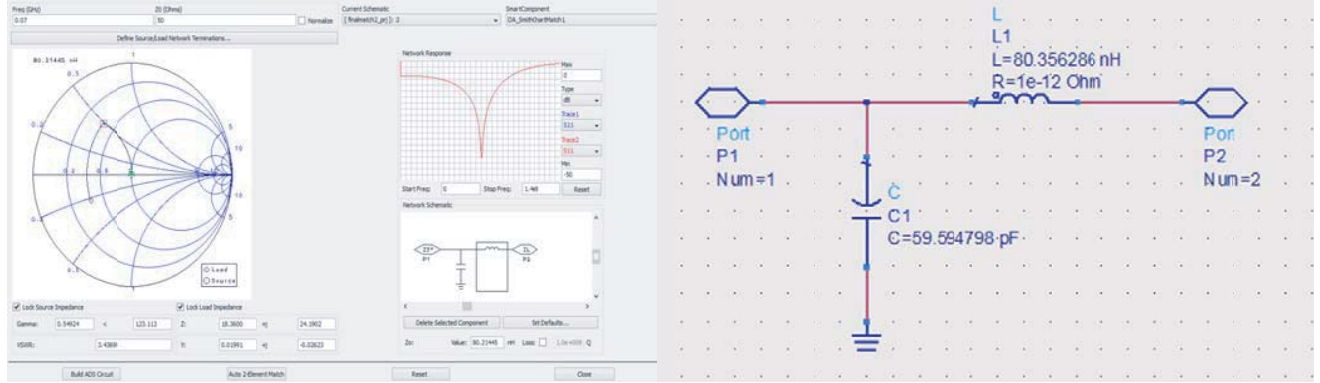
Figure 12. Impedance matching design for the 70 MHz RF to DC conversion circuit via ADS.
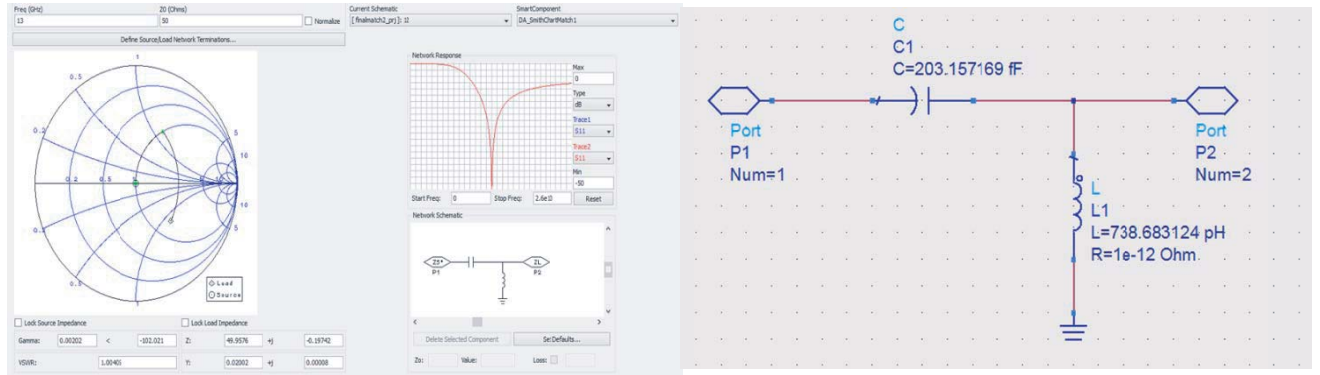

Figure 13. Impedance matching design for the 13 GHz RF to DC conversion circuit via ADS.

the highest voltage and gives it as an output. Since the 70 MHz and 13 GHz circuits give different outputs based on weather conditions, this power management ensures that the higher output is chosen for faster charging rate. The circuit was designed with overvoltage protection (V_{OV}) as well to avoid any damages to the circuit. The overvoltage resistor values $(R_{OV1} \& R_{OV2})$ were calculated using Equation (13) as below:

$$V_{OV} = V_{IN} \left(\frac{R_{OV1}}{R_{OV1} + R_{OV2}} \right) \tag{13}$$

The circuit also comes with a current limit protection (I_{LM}). The overcurrent resistor value (R_{ILM}) was calculated using Equation (14) as below:

$$I_{LM} = \frac{65.2}{R_{ILM0.861}} \tag{14}$$

Figure 14 shows the circuit design of the TPS2121 power management circuit.

Figure 15 shows the fabricated power management circuit and both the rectifier circuit output fed to the power management circuit.

The output of the power management circuit was then fed into a simple regulator circuit to produce a stable 5 V DC for smart phone charging. The regulator has a USB output port whereby end users will plug in their charger cable directly to this circuit. The LM577 voltage regulator is used to buck to high voltage output from the RF to DC conversion circuit. The fabricated regulator circuit is as shown in Figure 16.

5. RESULTS AND ANALYSIS

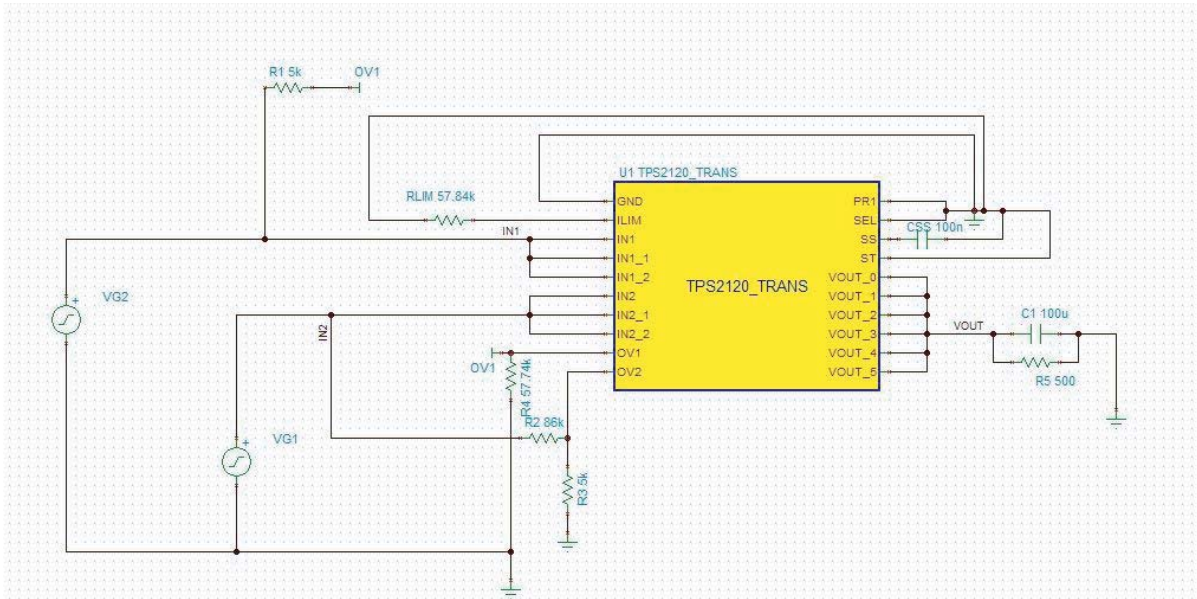This section will discuss the results and output of the RF harvesting circuits and its application.
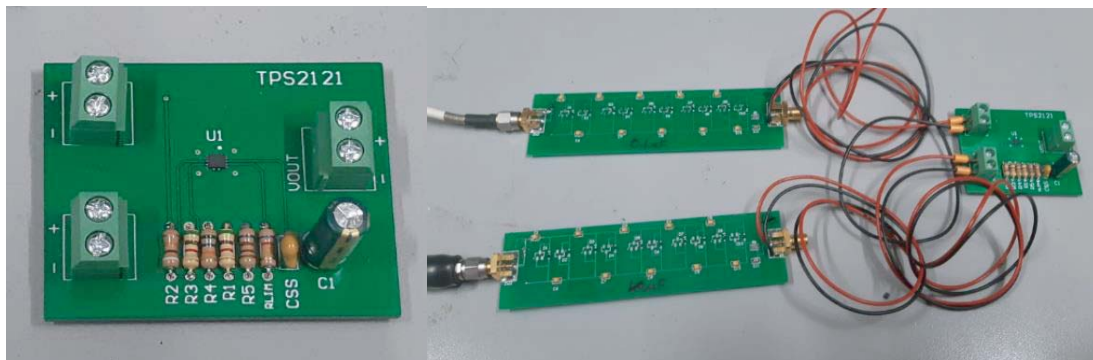
Figure 14. TPS2121 power management circuit.

Figure 15. Fabricated TPS2121 power management circuit with RF to DC conversion circuits.

5.1. Results via 2.4 GHz Wi-FI Energy Harvesting System

This section will discuss the results and output of the components involved in the RF energy harvesting via 2.4 GHz Wi-Fi signal.

5.1.1. Microstrip Patch Antenna Results

The antenna was tested under certain field conditions, and then results were captured accordingly. Figure 17 shows the return loss plot of the antenna.

It can be seen that the antenna resonates at a centre frequency of 2.451 GHz. This is within the operating frequency of the Wi-Fi band (2.4 GHz to 2.5 GHz). The return loss was observed at 33.18 dB, and the bandwidth is measured at 283 MHz. The antenna was tested in the data center of the broadcast station, and the following results in Table 4 are obtained.

The antennas were strategically placed in the data center to ensure that optimum RF energy is harvested. The received signal power is then fed into the rectifier circuit to produce a usable DC voltage. The matching network was also tested, and Figure 18 depicts the return loss of it.

It was observed that the matching network resonates at 2.4 GHz with a return loss of -46.39 dB. It also has a wide bandwidth of 800 MHz.
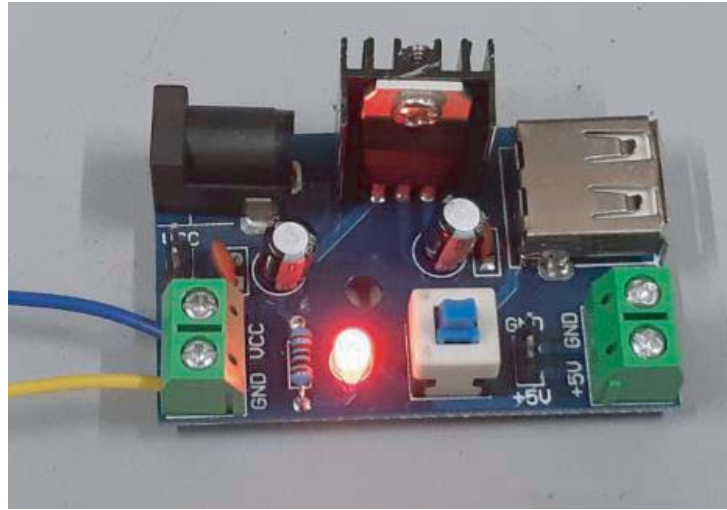
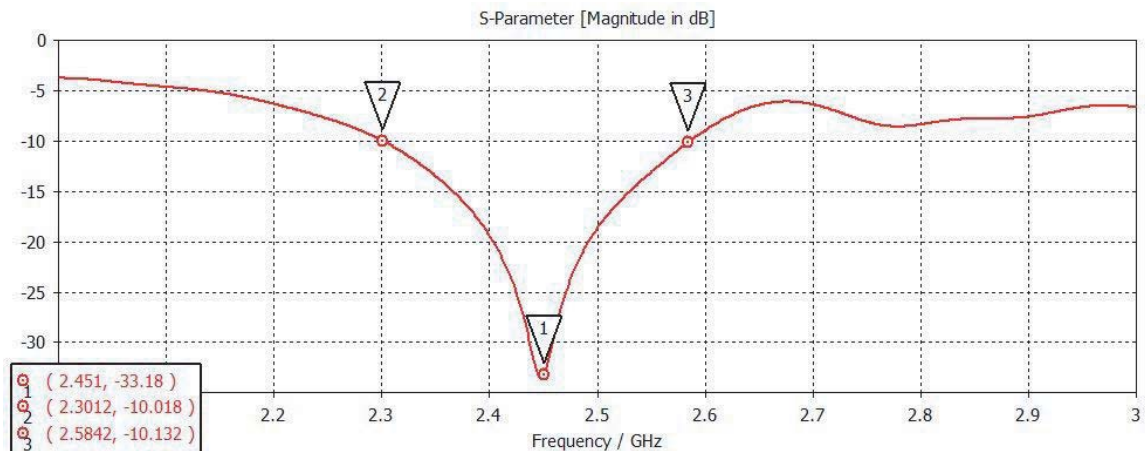**Figure 16.** Fabricated 5 V DC voltage regulator with USB output port.

Figure 17. S_{11} return loss plot of E-shaped microstrip patch antenna.

Table 4. Antenna test results.

Distance (cm)	Received signal power (dBm)	Received signal power (mW)
50	−4	0.398
100	−9	0.125
150	−17	0.019
200	−23	0.005

5.1.2. RF to DC Conversion Circuit Results

The 8-stage Villard voltage doubler was tested initially using a signal generator. A 2.4 GHz signal was pumped with the power level varied, and the output voltage was measured [14]. Besides that, the output signal from the microstrip patch antenna was connected to the voltage doubler circuit by varying the distance, and the output voltage was measured. The results are as shown in Table 5.

It was observed that the rectenna was able to produce sufficient output voltage. This is because of the efficient matching network designed which ensures maximum power transfer from the antenna to the
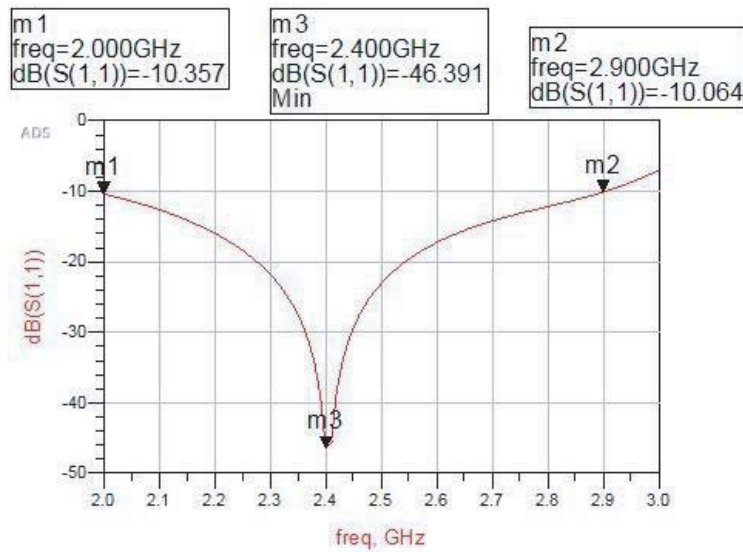
Figure 18. S_{11} return loss plot of the 2.4 GHz impedance matching circuit.

Table 5. RF to DC conversion circuit results.

Power level (dBm)	Simulation output (V)	Signal generator output (V)	Antenna output (V)
−5	1.29	1.55	1.34
−10	0.88	1.03	0.97
−15	0.55	0.77	0.63
−20	0.21	0.41	0.33

RF to DC conversion circuit. The simulation and signal generator outputs were lower than the actual antenna and rectifier circuit. The output from the rectenna is then fed into the power management circuit for further testing which is discussed in the next section.

5.1.3. Power Management Results

A 4.2 V Lithium Polymer (LiPO) battery is connected to battery charging port (VBAT) of the BQ25570. Once the boost controller is operating, it will constantly charge VBAT to 4.2 V. Once this is done, it will provide a constat output (V_{OUT}) of 3 V to the load. The rectenna circuit was plugged into the power management circuit, and the time taken for V_{STOR} to charge and to provide the regulated output was measured. Table 6 depicts the input voltage to the power management and the results of the power management.

The battery connected at V_{BAT} acts as a temporary backup when there is no incoming RF or DC. This was tested as well by disconnecting the input and allowing the battery to take over the system. The longer the battery is charged, the longer it can run the circuit and provide the 3 V regulated output to the load. Table 7 depicts the results of this test.

The longer V_{BAT} was charged, the longer V_{OUT} can provide a regulated output. In cases where the antenna or the RF to DC circuit is faulty or there is no incoming RF signal, the battery will be able to back up the system for a short period of time. The user would need to identify what went wrong and rectify as soon as possible to get the system up and running. The whole energy harvesting system was tested by connecting the TIDA-01398 motion sensor as load. The results are discussed in the next section.

Table 6. Power management results.

Input Voltage (V)	Time taken for V_{STOR} to charge (s)	Time taken for regulated output at V_{OUT} (s)
0.33	N/A	N/A
0.63	326	278
0.97	225	198
1.34	188	134

Table 7. Power management results without DC input.

Time VBAT was charged (s)	Time V_{OUT} was able to operate (s)
437	243
326	278
225	198
188	134

5.1.4. 2.4 GHz RF Energy Harvesting System Results

The whole system was connected and tested by powering up the TIDA-01398. This motion sensors were placed in the data centers and are connected to the lighting system of the area. When human presence is detected, the motion sensor sends a signal to the lighting system, and the lights in that area will be turned on. This is done as initiative for energy saving. The energy harvesting is connected to the motion sensor, and results were recorded based on the distance of the antenna to the RF source. Results are tabulated in Table 8.

Table 8. 2.4 GHz RF energy harvesting system results.

Distance (cm)	Received signal (dBm)	RF to DC output (V)	Time taken for V_{OUT} to operate (s)	Motion sensor operation
50	−4	1.34	134	Activated
100	−9	0.97	198	Activated
150	−17	0.63	252	Activated
200	−23	0.33	N/A	Not activated

It was noticed that at 200 cm from the antenna to the RF source, the motion sensor was unable to operate as the DC output is insufficient to cold start the BQ25570 to provide the regulated output to the motion sensor. The maximum distance for the motion sensor to be activated was at 184 cm. At this distance, the DC output was measured to be at 0.35 V. However, V_{STOR} took a very long time to start up the power management and allow V_{OUT} to operate. In order to ensure that the motion sensors are activated at all times, the antennas were optimally placed according to the available RF sources in order to have the best line of sight to harvest maximum RF power.

5.2. Results of RF Energy Harvesting via 70 MHz and 13 GHz

This section will discuss the results and output of the circuitries involved in the RF energy harvesting via the 70 MHz and 13 GHz signal.

5.2.1. LC Matching Network Circuits Results

As discussed earlier, two LC matching networks were designed for the 70 MHz and 13 GHz RF to DC conversion circuits. The return loss plot in Figure 19 shows the results of the matching network designed for the 70 MHz and 13 GHz circuits, respectively.
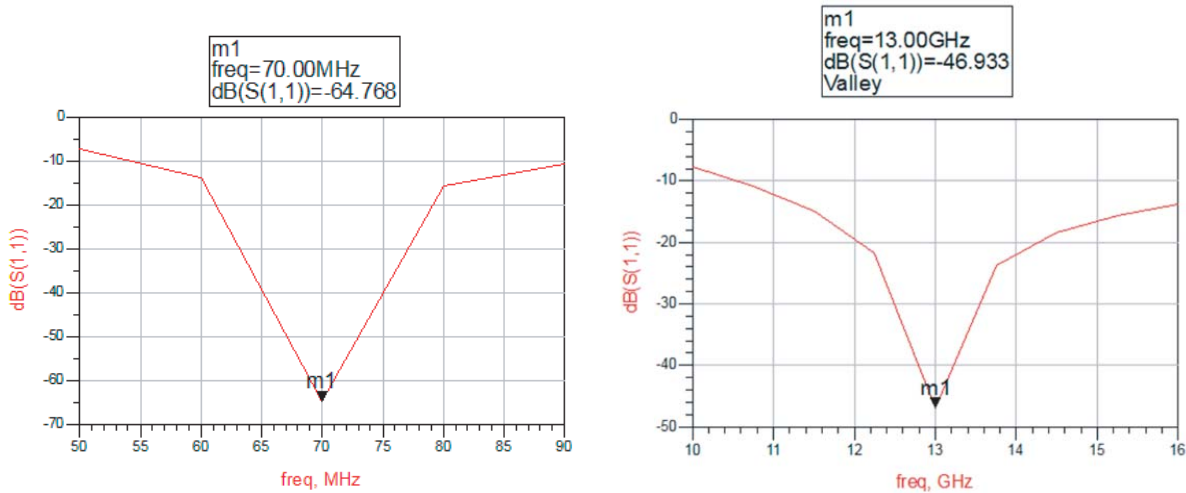

Figure 19. Return loss plots for 70 MHz and 13 GHz LC matching network circuits.

For the 70 MHz circuit, the return loss was recorded at −64.768 dB, and the bandwidth is at 40 MHz. For the 13 GHz circuit, the return loss was measured at −46.933 dB, and the bandwidth is at 4 GHz. The rectifier circuit was tested with and without the LC matching network circuit, and the output seemed to be improved with the matching network. The results of this are discussed in the next section.

5.2.2. RF to DC Conversion Circuit Results

The RF to DC conversion circuit was initially tested with a signal generator by pumping in 70 MHz and 13 GHz signals. Power levels were varied in order to test the performance of the circuit. The circuits were tested with and without matching networks. Table 9 shows the results of the 70 MHz and 13 GHz RF to DC conversion circuit.

The results show that the RF to DC conversion circuit had better efficiency with the LC matching network circuit as the loss is minimal due impedance matching and allows proper power transfer. At

Table 9. 70 MHz & 13 GHz RF to DC conversion circuit results.

Power level (dBm)	DC output without matching network (V)		DC output with matching network (V)	
	70 MHz	13 GHz	70 MHz	13 GHz
−5	3.4	0	5.2	0
0	5.8	0	7.6	0
5	8.7	0	10.2	0
10	12.4	2.3	18.2	3.6
20	N/A	8.7	N/A	13.4
30	N/A	19.8	N/A	23.1

+10 dBm, the 70 MHz circuit produces a DC output of 18.2 V. The circuit was not further tested with higher power levels as the diodes maximum input power level is at +10 dBm. At lower power levels, the 13 GHz circuitry was unable to produce any DC output as it suffers major loss due to the high frequency. At +30 dBm, the 13 GHz circuit produced a DC output of 23.1 V. This DC outputs are fed into the power management circuit and finally regulated to 5 V. Sufficient amount of current is produced for smart phone charging when these high voltage outputs are stepped down to 5 V at the final stage.

5.2.3. Power Management Circuit Results

The TPS2121 power management circuit switches to higher power supply seamlessly, and this was initially tested using a DC power supply. Later, the RF to DC conversion circuit was connected to the TPS2121 circuit and was tested. The first input ($V1$) of the TPS2121 was connected to the 70 MHz circuit, and the second input ($V2$) was connected to the 13 GHz input.

The overvoltage protection of the first input was designed to be at 18 V, and the second input overvoltage was at 24 V as reference to the results of the RF to DC circuits at +10 dBm for the 70 MHz circuit and +30 dBm for the 13 GHz circuit. The circuit was tested by connecting to a DC power supply, and the overvoltage protection was noticed working fine. Both the 70 MHz and 13 GHz circuits were then connected to the TPS2121 circuit as shown in Figure 20.
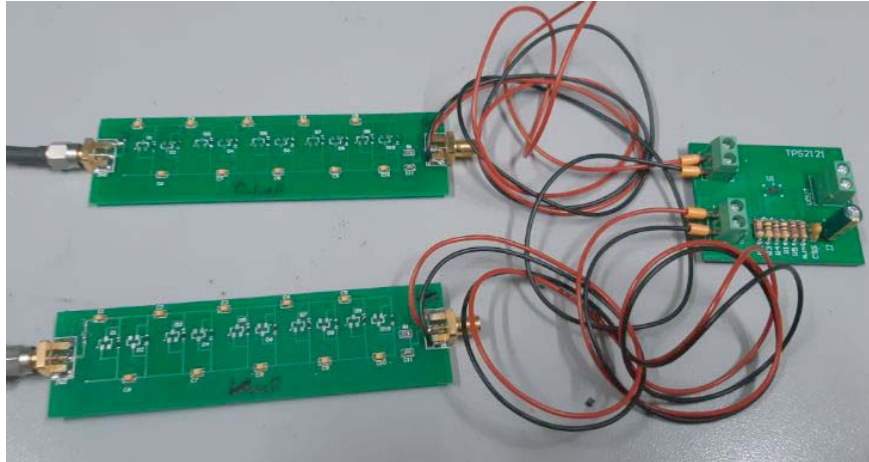

Figure 20. 70 MHz and 13 GHz RF to DC conversion circuits connected to TPS212.

The power management circuit was tested by varying the power level to the input of the RF to DC circuits. This is done by using the signal generator. The results are tabulated in Table 10.

It was noticed that initially $V1$ is the active output as the voltage is higher than $V2$. Once the

Table 10. Power management results.

Power level (dBm)	DC output (V)		Active output
	70 MHz ($V1$)	13 GHz ($V2$)	
−5	5.2	0	$V1$
0	7.6	0	$V1$
5	10.2	0	$V1$
10	18.2	3.6	$V1$
20	N/A	13.4	$V1$
30	N/A	23.1	$V2$

voltage on $V2$ rises, the circuit automatically switches to $V2$ and outputs it to the load. Once $V2$ decreases, the circuit automatically switches back to $V1$ and maintains at it until a rise is noticed on $V2$. The RF to DC circuit was then connected to the uplink transmission path, and the same was observed. During clear sky operations, the 70 MHz RF to DC output is used to power up the load. When it rains, the 13 GHz RF to DC output is higher, and the power management selects this voltage instead to power up the load.

5.2.4. RF Energy Harvesting via 70 MHz and 13 GHz Results

The RF to DC conversion circuits were connected to the TPS2121 power management circuit. The output of the TPS2121 was connected to the voltage regulator. A smart phone was plugged to the USB output of the voltage regulator circuit. For testing purposes, the Samsung Galaxy A8 phone was used to test the charging rate. This phone has fast charging capability, and the nominal current required for this is 2 A. However, the RF energy harvesting circuit will not be able to produce such high currents, hence a slow but acceptable charging rate is expected. The system was tested, and the results are tabulated in Table 11.

Table 11. RF energy harvesting via 70 MHz and 13 GHz results.

Input	DC output (V)	Regulated DC output (V)	Current (A)	Time taken to fully charge (min)
70 MHz at +10 dBm	18.2	5	0.3	123
13 GHz at +30 dBm	23.1	5	0.5	84

From the results measured, it can be seen that the 13 GHz circuit provides a better current output and in return has a faster charging rate than the 70 MHz circuit. The current is approximately 0.5 A which is the same as any USB charging port available on laptops, TV, or any other devices. The time taken to fully charge the handphone is quite high compared to a normal charger as the current is lower, and in return a slower charging rate is expected.

Users can temporarily use this charging facility in case of emergency or for backup if they have misplaced their charger. This is somehow a form of renewable energy available 24×7 whereby unused coupler outputs of RF energy are converted into usable DC power which is used for smart phone charging. Especially during this era where smart phones are an essential, this charging facility will definitely benefit the end users.

6. CONCLUSION

In conclusion, two types of RF energy harvesting systems are designed and implemented in a broadcast station. First is the 2.4 GHz energy harvesting system placed in the data center which is used to power up motion sensors connected to the lighting system in the area. An E-shaped microstrip path antenna is placed 185 cm away from its source, producing a DC voltage of 0.35 V, which is sufficient to start up the BQ25570 power management circuit. The BQ25570 then provides a constant 3 V regulated output to power up the TIDA-01398 motion sensor and charges a 4.2 V LiPO rechargeable battery simultaneously. In case there is no incoming RF or DC, the battery can be used as a temporary backup to power up the system.

The second energy harvesting system consists of the 70 MHz signal from the modulator and 13 GHz from the high-power amplifier derived from the uplink system. LC matching networks were designed, and the DC outputs were connected to the TPS2121 power management circuit which selects the higher DC input. During normal operation, the 70 MHz is expected to charge the smart phone at charging rate of 0.3 A. During rain, the high-power amplifier will have a higher output, and the 13 GHz circuit is expected to charge the smart phone at a charging rate of 0.5 A. Compared to other studies, this work has excelled in harvesting from high frequency and also to use the converted DC for smart phone charging instead of other low power application. Increasing the charging rate is something to be looked into for future researches.

ACKNOWLEDGMENT

REFERENCES

1. Diagarajan, M. S., A. Ramasamy, N. B. M. Din, and P. N. Vummadisetty, "A review on the contemporary research on radio frequency energy harvesting," *International Journal of Engineering and Technology (UAE)*, Vol. 7, No. 3, 52–58, 2018.

2. Alneyadi, F, M. Alkaabi, S. Alketbi, S. Hajraf, and R. Ramzan, "2.4 GHz WLAN RF energy harvester for passive indoor sensor nodes," *Proc. 2014 IEEE International Conference on Semiconductor Electronics (ICSE)*, 471–474, Aug. 27–29, 2014.

3. Mikeka, C. and H. Arai, "Design issues in radio frequency energy harvesting system," *Sustainable Energy Harvesting Technologies — Past, Present and Future*, Dec. 2011.

4. Pinuela, M., P. D. Mitcheson, and S. Lucyszyn, "Ambient RF energy harvesting in urban and semi-urban environments," *IEEE Transactions on Microwave Theory and Techniques*, Vol. 61, No. 7, 2715–2726, Jul. 2013.

5. Diagarajan, M. S., A. Ramasamy, N. Boopalan, and N. B. M. Din, "RF energy harvesting prototype operating on multiple frequency bands with advanced power management," *Indonesian Journal of Electrical Engineering and Computer Science*, Vol. 17, No. 1, 70–77, 2019.

6. Adami, S.-E., C. Vollaire, B. Allard, F. Costa, W. Haboubi, and L. Cirio, "Ultra-low power autonomous power management system with effective impedance matching for RF energy harvesting," *2014 8th International Conference on Proc. Integrated Power Systems (CIPS)*, 1–6, Feb. 25–27, 2014.

7. Diagarajan, M., A. Ramasamy, N. M. Din, and K. K. A. Devi, "Comparison on microstrip patch antenna modules and rectifier modules for RF energy harvesting," *ARPN Journal of Engineering and Applied Sciences*, Vol. 11, No. 10, 6228–6233, 2016.

8. Yi, J., W. Ki, and C. Tsui, "Analysis and design strategy of UHF micro-power CMOS rectifiers for micro-sensor and RFID applications," *IEEE Trans. Circuits Syst.*, Vol. 54, No. 1, 153–166, Jan. 2007.

9. Kong, N. and D. S. Ha, "Low-power design of a self-powered piezoelectric energy harvesting system with maximum power point tracking," *IEEE Transactions on Power Electronics*, Vol. 27, No. 5, 2298–2308, May 2012.

10. Sedeek, A., E. Tammam, and E. Hasaneen, "High efficiency 2.45 GHz low power hybrid junction rectifier for RF energy harvesting," *2018 International Japan-Africa Conference on Electronics, Communications and Computations (JAC-ECC)*, 147–150, Alexandria, Egypt, 2018.

11. Pulvirenti, F., A. La Scala, D. Ragonese, K. D'Souza, G. M. Tina, and S. Pennisi, "4-phase interleaved boost converter with IC controller for distributed photovoltaic systems," *IEEE Transactions on Circuits and Systems I: Regular Papers*, Vol. 60, No. 11, 3090–3102, Nov. 2013.

12. Devi, K. K. A., M. D. Norashidah, C. K. Chakrabarty, and S. Sadasivam, "Design of an RF-DC conversion circuit for energy harvesting," *Proc. 2012 IEEE International Conference on Electronics Design, Systems and Applications (ICEDSA)*, 156–161, Kuala Lumpure, Nov. 5-6, 2012.

13. Diagarajan, M., A. Ramasamy, N. M. Din, and K. K. A. Devi, "Comparison on microstrip patch antenna modules and rectifier modules for rf energy harvesting," *ARPN Journal of Engineering and Applied Sciences*, Vol. 11, No. 10, 6228–6233, 2016.

14. Sedeek, A., E. Tammam, and E. Hasaneen, "High efficiency 2.45 GHz low power hybrid junction rectifier for RF energy harvesting," *2018 International Japan-Africa Conference on Electronics, Communications and Computations (JAC-ECC)*, 147–150, Alexandria, Egypt, 2018.